Nitrogen atmospheric pressure post discharges for biological decontamination of inside small diameter tubes

Anne-Marie Pointu, André Ricard, Emmanuel Odic, Mihai Ganciu

Nitrogen Atmospheric Pressure Post Discharges for Surface Biological Decontamination inside Small Diameter Tubes

Anne-Marie Pointu,* André Ricard, Emmanuel Odic, Mihai Ganciu

A nitrogen afterglow at atmospheric pressure has recently been described as able to transport active species over long distances in small diameter tubes, with a biocidal effect. For a discharge gas composed of nitrogen, either of high purity or with some controlled ppm of oxygen, survival curves are presented. The afterglow, flowing at 40 slm in a cylindrical quartz tube with 8 mm internal diameter is studied using emission spectroscopy. Fundamental or excited states of atomic or molecular species of parent gases are detected and evaluated. Their absolute concentration is measured along the tube axis. Correlated to transport equations, results give information on the creation and destruction reactions of these species, especially of the $O(^1S)$ metastable state of O, the species that has been shown to boost the biocidal effect.
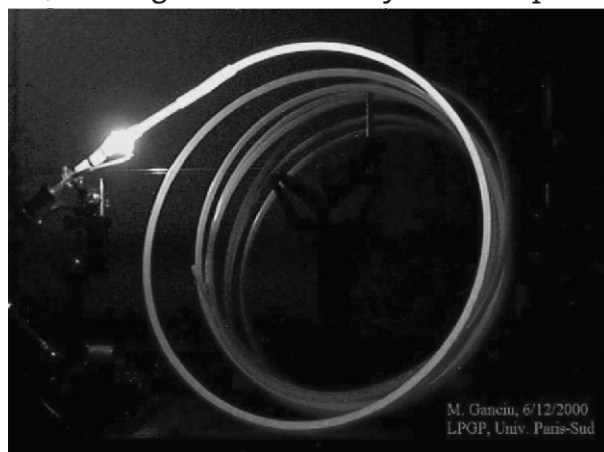
Introduction

Among plasma methods used to inactivate microorganisms, those based on atmospheric pressure discharges and remote exposure are numerous, because of the practical simplicity and thermo-sensitive medium preservation.

In particular, devices have been developed under different configurations to produce cold effusing plasma jets or plumes able to treat surfaces in ambient air.[1,2]

A.-M. Pointu, M. Ganciu
Laboratoire de Physique des Gaz et des Plasmas, Bat 210, Université Paris-Sud, 91405 Orsay Cedex, France
E-mail: anne-marie.pointu@u-psud.fr
A. Ricard
Laplace, Université Paul Sabatier, 31062 Toulouse Cedex 9, France
E. Odic
Département Energie, SUPELEC, 91192 Gif-sur-Yvette Cedex, France

Worth mentioning among the alternative approaches that use direct exposure or lower pressure, are floating electrode dielectric barrier discharges (DBDs)[3] or low pressure afterglow sterilizers, and flowing microwave discharge as presented in ref. [4]; the latter appears promising to treat the interior surface of narrow bore tubes.

Two ambitious and useful objectives are concerned with here, they are the sterilization of the inside of poly-(ethylene terephthalate) (PET) capillary tubes of different shapes and lengths and decontamination of flow tubes, both for medical and domestic applications. To achieve these objectives, a possible approach is to use the chemical activity of the 'species' produced in a discharge and transported to the surface to be treated. Again, at atmospheric pressure, active species can be transferred in the discharge effluent[5] or, as presented in this paper, in the discharge following flowing afterglow.

A device that has the unique capability of propagating nitrogen atoms over long distances in small diameter tubes has been studied for several years at the Orsay Plasma Lab. Its biological decontamination efficiency has been demonstrated and attributed to specific atoms and molecules produced by the discharge. Major results shall be discussed and a spectroscopic study shall be presented in order to understand the kinetics involved, the goal being to optimize the biocidal effect.

Experimental Set-Up

An atmospheric pressure nitrogen afterglow has already been described elsewhere.[6–8] It flows at about 40 standard liters per minute (slm) from successive fast pulsed corona discharges produced between needles with a voltage of some 10 kV, a repetition rate of some 10 kHz, and a mean power near 15 W. When contained in a manuril tube (6 mm inner diameter), it produces external fluorescence over more than 10 m, as shown in Figure 1(a).
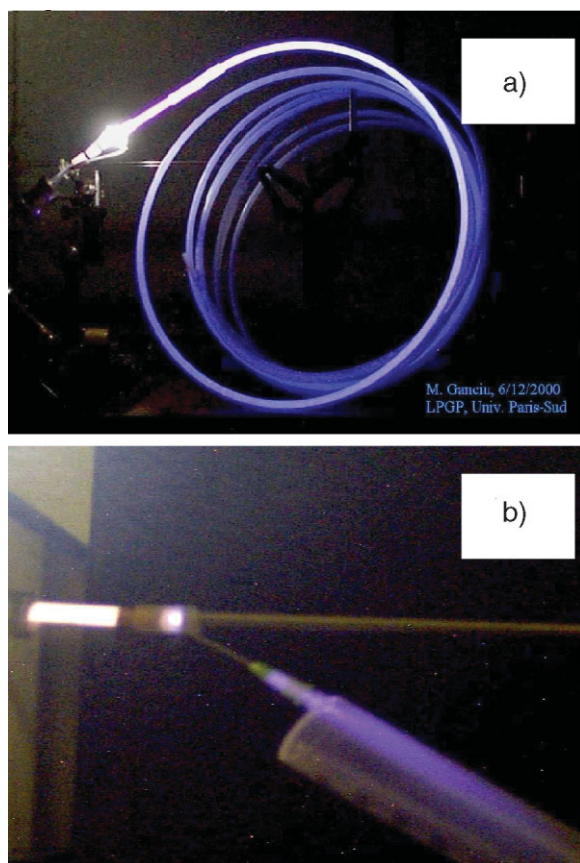
Figure 1. Atmospheric nitrogen flowing post discharge (flow around 40 slm): a) producing fluorescence of a manuril tube, internal diameter 6 mm, over more than 10 m; b) extracted from a manuril tube through a syringe needle.

Gas luminosity is observable to the eye, even some centimeters in length downstream of a syringe needle (see Figure 1(b)).

Such light emissions have been attributed to transported nitrogen atoms. In fact, a high impedance regime of each corona discharge before it is swept out by the gas flux is able to give a high dissociation efficiency to the discharge. Moreover, the gas temperature is around 300 K, as shown by comparison of measured and simulated spectra.[9]

Thus, in view of the pursued applications, we shall study cylindrical post discharge, both by measuring contained 'active' species using spectroscopic means and by testing their biocidal effects.

A typical experimental set up is shown in Figure 2. High purity N_2 gas (99.995%) is introduced upstream of the discharge and, in parallel, a small proportion of O_2 can be added as a controlled impurity. Two flow controllers adjust the corresponding flows respectively to 40 slm and to 0–50 standard cubic centimeters per minute (sccm). Downstream of the discharge region, the afterglow is established in a quartz tube of 8 mm internal diameter, ending in atmospheric air. The emission spectroscopy device (ROPER SCIENTIFIC) is composed of an ACTON spectrometer (0.25 nm resolution with 1 200 lines) and a CCD PIXIS-100 detector working from 200 to 1 080 nm. The spectrometer entrance slit is coupled to one end of an optical fiber of 400 μm diameter through a filter used to eliminate higher order interference. The other end of the fiber, covered with a quartz lens, is movable in parallel with the discharge axis. The spectroscopic acquisition time is around 20 s.

When necessary, biocidal tests were performed, interposing a 250 cm³ plastic box that contained biological species, 10 cm downstream of the discharge region. Two types of microorganisms have been used for surface decontamination tests. i) *Bacillus stearothermophilus* (spore suspension CIP# 52.82 from Institut Pasteur) was used in the experiments reported here. These bacteria cells are used in their resistant form (spores), i.e., dehydrated and protected by protein shells that insulate the microorganism core from the environment. ii) *Escherichia coli* DH1 strain was also selected as the bacterial model and stored at −20 °C in glycerol (20%, v/v). Bacteria were subcultured at 30 °C for 20 h in M63 minimal medium supplemented with glucose (0.2%) without agitation for all experiments.

For the decontamination tests, the methods described in the two following paragraphs were used.

The initial *B. stearothermophilus* spore suspension ($\approx 2 \times 10^7$ spores · mL^{-1}) was first diluted (1/10) in distilled water and 10 μL droplets from this diluted suspension were deposited on sterile glass slides (circular slides of 12 mm diameter). The glass slides, bearing
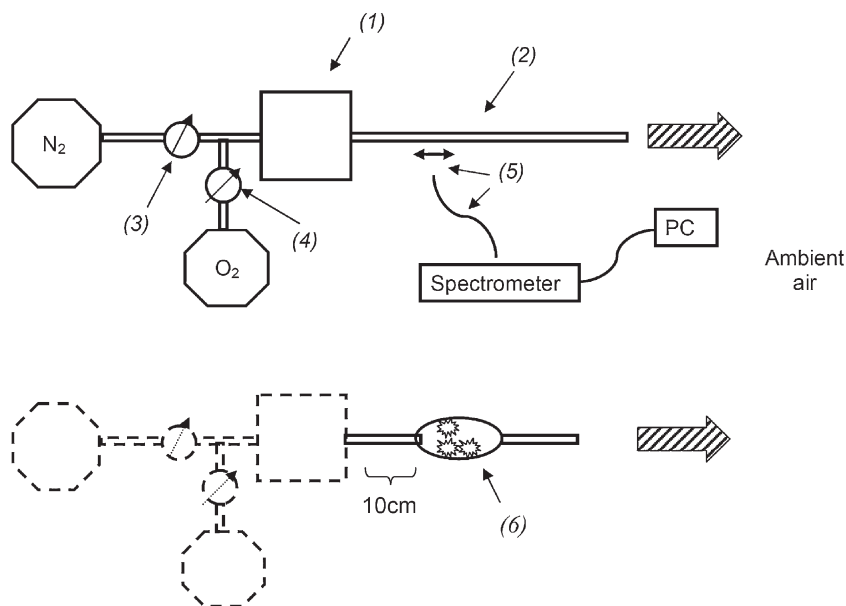
Figure 2. Experimental set up. (1): discharge box; (2) quartz post discharge tube, 8 mm internal diameter 1 m long; (3) and (4): flow controllers for respective fluxes of 0–50 slm N_2 and 0–50 sccm O_2; (5): optical fiber and lens; (6): box containing microorganisms.

$\approx 2 \times 10^4$ spores on their surface, were then dried in an incubator at 40 °C for 30 min in order to evaporate the distilled water.

An overnight *E. coli* culture was centrifuged (4 000g, 10 min) and the cells were re-suspended in physiological solution. A first optical titration ($OD_{600nm} = 1$) corresponding to 10^9 cells per mL was performed. After successive dilutions, the concentration was tested by colony counting. Droplets of 10 µL of the cell suspension that contained $\approx 10^6$ cells were deposited on sterile glass slides and dried at room temperature for 45 min prior to plasma treatment.

For each experimental condition (varying gas composition, exposure time) tested, five slides were prepared, i.e., four submitted to the plasma flowing afterglow (at the tube outlet in the 250 cm^3 box), and one stored in the lab atmosphere for the same duration, as a control. Note that another control experiment was performed in which samples were placed into the treatment box and submitted to the same gas flow conditions, except with the plasma turned off; the same result was obtained as that for the fifth slide control.

After treatment, microorganisms from each slide (treated and control) were collected (5 min of sonication of each glass slide in a 2 mL volume of distilled water for *B. stearothermophilus* and successive recuperations in a 2 mL total volume of physiological solution for *E. coli*). The obtained suspensions were serially diluted and then plated out (100 µL) on an agar surface (Petri dish) for enumeration of microorganisms by a direct plate counting method.

Direct counting was done after a 36 h incubation period at 56 °C and a 12 h incubation period at 37 °C for *B. stearothermophilus* and *E. coli*, respectively. Note that appropriate dilutions were made according to i) the expected number of survivors and ii) the reliability of the CFUs (colony forming units) counting, i.e., single isolated bacteria form visible isolated colonies in a statistically significant range (30–300 colonies per plate).

The decontamination efficiency results are presented on semi-logarithmic graphs called 'survival curves' where $\log_{10}$ of the number of survivors is plotted as a function of the exposure time.

Preliminary Concentration Measurements

Emission spectra are used to identify the species present, X, and to deduce their concentration, denoted [X] (cm^{-3}). As previously described in ref. [7] from a study with a lower resolution spectrometer, emissions surprisingly appear in visible region bands from CN (359, 388, and 424 nm) and from NH (336 nm), which have been attributed to hydrocarbon impurities in the nitrogen supply reacting with nitrogen atoms. The nitrogen spectrum in the plasma as well as in the flowing afterglow is mainly composed of the molecular first positive (1st pos), including the 580 nm band. This band comes from the $N_2(B, v' = 11)$ state which originates from recombination of two $N(^4S)$ atoms (also noted N, for simplicity), and thus is proportional to $[N]^2$. When adding small quantities of O_2, as shown in ref. [7], the observed spectrum is completely changed, with NO_γ and NO_β bands appearing in the place of the vanished CN and NH bands. The NO_γ UV band is particularly interesting around 250 nm, which is known to be biocidal. At 557 nm, for a specific O_2/N_2 ratio range, the 'auroral' line, a signature of the $O(^1S)$ state, also appears.

In order to overcome the difficulty of unknown absolute sensitivity of the spectrometer device, [N] was measured with a new method using titration with O_2,[9] and results have been compared to N transport modelling.[10]

Results obtained in previous manuril tube experiments for distances downstream of the discharge ranging from 10 cm to 3 m showed that [N] decreases from 3×10^{14} cm^{-3} to 3×10^{13} cm^{-3}, with losses during transport a result of recombination alone. It was shown that recombination in the bulk volume is dominant in the first 20 cm of transport length, the influence of surface recombination appearing further downstream.

[N] being known, it was then possible to calibrate the spectrometer device. This calibration allowed, in particular, the measurement of [O(^{1}S)] from the auroral line.[7]

Biocidal Effects

In pure nitrogen, two types of microorganisms have been used for surface decontamination tests: *E. coli* bacteria and *B. stearothermophilus* spores.

Survival curves are reproduced in Figure 3(a) and 3(b). They demonstrate that there is a biocidal effect in pure nitrogen. This effect is high in the case of bacteria (population reduction approaching 3 decades in 5 min), and much lower but nevertheless existent for spores.

Despite the less effective results, the use of spores is preferred because they present a very low probability of damage during their manipulation, and because they are currently used for inactivation tests of wet heat sterilization processes (autoclave).

In order to evaluate the impact of an O_2 admixture in N_2 on the decontamination efficiency, tests have been carried out using either 'pure' nitrogen (Alphagaz 2 from Air Liquide: $H_2O < 0.5$ ppm, O_2, CO, CO_2, C_nH_m, and $H_2 < 1$ ppm) or nitrogen with oxygen introduced as an impurity. Results are presented in Figure 4 where the survival curve using pure nitrogen exhibits a biocidal effect which can be only attributed to N. The latter curves obtained with oxygen
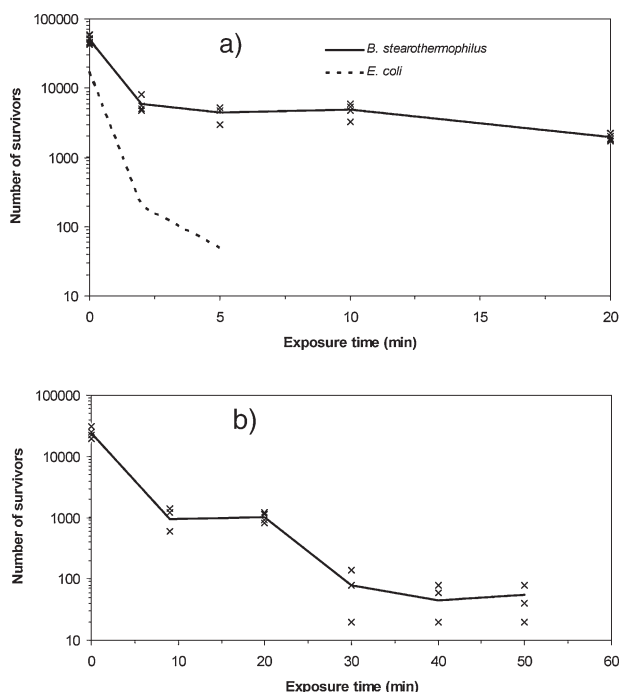

Figure 4. Effect of O_2 admixture in N_2 on survival curves; $+$ and ——: pure N_2; $\bigcirc$ and - - -: admixture of 25×10^{-5} O_2; $\triangle$ and -----: admixture of 2.5×10^{-5} O_2.

impurities studied in ref. [7] have been related to possible biocidal agents: UV, O(^{1}S), and N, respectively quantified by 248, 557, and 580 nm bands. It was concluded that metastable O(^{1}S) coupled to N were the most efficient species to inactivate *B. stearothermophilus* spores.

Finally, the device under study appears to be efficient in the decontamination of the interior surface of tubes. A correlative study on medical catheters[a] demonstrated that, in the case of pure nitrogen, no significant degradation of the polyurethane wall surface was observed. The same study in the case of an O_2 admixture is yet to be done.

It is thus important to understand the creation, loss, and transport of active species along the tube and, more generally, to identify and measure all possible metastable states.

Basis of Spectroscopic Measurements

Observed Bands/Lines and Deducible Concentrations

Using the spectroscopic device, the following bands and lines, noted by their wavelength (λ) shall be studied: 248 nm (NO$_\gamma$ band), 320 nm (NO$_\beta$ band), 557 nm (auroral green line), 580 nm (N_2 first positive band). The upgraded spectrometer sensitivity also permits the study of the 346.6 nm N(^{2}P $\rightarrow$ ^{4}S) forbidden line (see Figure 5) only visible in pure N_2.

Table 1 presents the creation and loss reactions (with their considered line and band emissions) of each upper radiative state.

Figure 3. Survival curves in pure nitrogen post discharge: a) comparison for two types of biological species; b) case of spores for longer exposure time range.
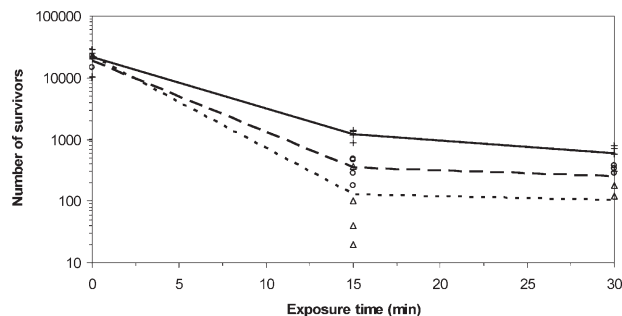
---

a This study was the subject of a thesis defended in 2007 by O. Mrad (Faculty of Pharmacology, Paris XI University) in the frame of a PPF network. It is shown that polymer chains do not present scission nor reticulation and that their organization into the matrix is not affected. Neither polymer oxidation, nor degradation, nor migration properties of the contained additives are observed. The only noticed effect is a reversible increase of surface polarity. The bacterial adhesion capacity is not affected.
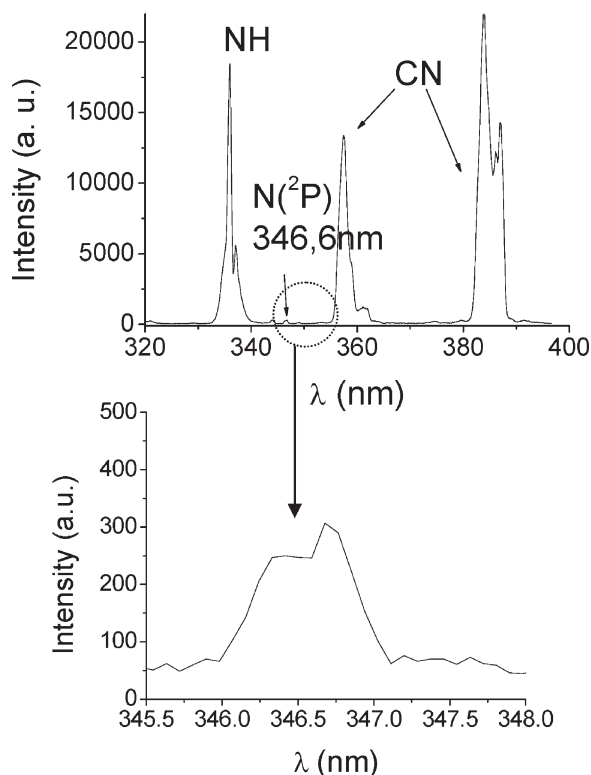
Figure 5. Observation of the forbidden line $\lambda = 346.6$ nm from N(^{2}P) metastable state.

Convection is considered negligible in the excited state concentration balance. Such an assumption is easy to check for reasonableness, for radiating states (580, 248,

320 nm), and even for conditions of high gas velocity (around $1\,300$ cm $\cdot$ s^{-1}).

The case of the auroral line, which is emitted by the radiating O(^{1}S)N$_2$ excimer state, involves metastable O(^{1}S) only through a quasi-equilibrated reaction presented in Table 1 (see ref. [15]). Convection is thus shown to be negligible.

Finally, the case of the forbidden line at 346.6 nm, which originates from the 3.57 eV metastable N(^{2}P) has to be examined. This shall be done, a posteriori, after calculations assuming negligible convection.

Table 1 presents the reactions, denoted (1) to (10), involved in species creation and loss. Using the listed spectroscopic emissivity and reaction constants, and for $[N_2] = 2.42 \times 10^{19}$ cm^{-3}, measured line intensities I(nm) can be related to local concentrations:

$$I(580) = P_1\,[N]^2 \qquad P_1 = 2.8 \times 10^{-18} \times b \times G(580)/580$$
$$I(557) = P_2\,[O(^1S)] \qquad P_2 = 96.8 \times b \times G(557)/557$$
$$I(248) = P_3\,[NO] \times [N_2(A)] \qquad P_3 = 3.6 \times 10^{-11} \times b \times G(248)/248$$
$$I(322) = P_4\,[N] \times [O] \qquad P_4 = 1.34 \times 10^{-17} \times b \times G(322)/322$$
$$I(346.6) = P_5\,[N_2(A)] \times [N] \qquad P_5 = 1.49 \times 10^{-19} \times b \times G(346)/346$$
$$I(346.6) = P_6\,[N(^2P)] \qquad P_6 = 5.4 \times 10^{-3} \times b \times G(346)/346$$

G(nm) is the relative spectroscopic sensitivity of the measurement device and b is an unknown coefficient, shared by all constant coefficients P_i, making a calibration necessary. Because of the potential importance of excited species, either atomic or molecular, I(346.6) has been expressed both as a function of the upper level

Table 1. Creation and main loss reactions of studied upper radiative states

Studied band/line	Upper radiative state production	Main upper radiative state loss
$N_2(B, 11) \rightarrow N_2(A, 7) + \lambda(580\text{ nm})$ ($A(580) = 7.76 \times 10^4$ s^{-1} [7])	$N + N + N_2 \rightarrow N_2(B, 11) + N_2$ (1) ($k_1 = 1 \times 10^{-33}$ cm$^6 \cdot$ s^{-1} [7])	$N_2(B, 11) + N_2 \rightarrow$ products (2) ($k_2 = 2.8 \times 10^{-11}$ cm$^3 \cdot$ s^{-1} [7])
$NO(A, 0) \rightarrow NO(X, 2) + \lambda(248\text{ nm})$ ($A(248) = 1.124 \times 10^6$ s^{-1} [11])	$N_2(A) + NO \rightarrow NO(A, 0) + N_2$ (3) ($k_3 = 6.6 \times 10^{-11}$ cm$^3 \cdot$ s^{-1} [12])	$NO(A, 0) \rightarrow NO(X) + h\nu$ (4) ($A_4 = 4.9 \times 10^6$ s^{-1} [11]) $NO(A, 0) + N_2 \rightarrow$ products (5) ($k_5 = 4.9 \times 10^{-14}$ cm$^3 \cdot$ s^{-1} [12])
$NO(B, 0) \rightarrow NO(X, 8) + \lambda(322\text{ nm})$ ($A(322) = 8.513 \times 10^4$ s^{-1} [13])	$N + O + N_2 \rightarrow NO(B, 0) + N_2$ (6) ($k_6 = 2.9 \times 10^{-34}$ cm$^6 \cdot$ s^{-1} [14])	$NO(B, 0) + N_2 \rightarrow$ products (7) ($k_7 = 6.1 \times 10^{-13}$ cm$^3 \cdot$ s^{-1} [14])
$N_2 \cdot O(^1S) \rightarrow N_2 \cdot O(^1D) + \lambda(557\text{ nm})$ ($A(557) = 4 \times 10^{-18} \times k_{8inv}/k_{8dir}$ s^{-1} [15])	$O(^1S) + N_2 + N_2 \leftrightarrow N_2 \cdot O(^1S) + N_2$ (8) (k_{8dir} (direct) and k_{8inv} (inverse))	
$N(^2P) \rightarrow N + \lambda(346.6\text{ nm})$ ($A(346.6) = 5.4 \times 10^{-3}$ s^{-1} [16])	$N_2(A) + N \rightarrow N_2 + N(^2P)$ (9) ($k_9 = 4 \times 10^{-11}$ cm$^3 \cdot$ s^{-1} [17])	$N(^2P) + N_2 \rightarrow N + N_2$ (10) ($k_{10} = 6 \times 10^{-14}$ cm$^3 \cdot$ s^{-1} [17])

population and as a function of the species producing this state.

Spectroscopic Calibration

As previously mentioned, bulk volume recombination dominates the N loss process in the first tens of centimeters downstream of the discharge and wall recombination does not affect the linearity of the 1/[N] curve versus axial distance, z, which corresponds with the solution of the density conservation equation:

$$V d[N]/dz = -2\alpha_{eff} \times [N]^2 \times [N_2] \qquad (11)$$

V, the flow velocity, is here equal to $1\,333 \text{ cm} \cdot \text{s}^{-1}$. In fact when the wall recombination probability, γ, is zero, $\alpha_{eff} = \alpha_0 = 4.4 \times 10^{-33} \text{ cm}^6 \cdot \text{s}^{-1}$ (rate of volume reaction[18])

$$N + N + N_2 \rightarrow 2N_2 \qquad (12)$$

Thus, at the beginning of spatial afterglow, it shall be considered that the solution of Equation (11) is:

$$1/[N] = 1/[N]_0 + (2\alpha_0[N_2]/V)z \qquad (13)$$

giving, with P_1 as defined previously:

$$\frac{1}{\sqrt{I(580)}} = \frac{1}{\sqrt{P_1}}\left(\frac{1}{[N]_0} + \frac{2\alpha_0[N_2]}{V}\right)z \qquad (14)$$

The corresponding $1/\sqrt{I(580)}$ curve versus z is a straight line whose measurable slope is equal to $\frac{1}{\sqrt{P_1}}\frac{2\alpha_0[N_2]}{V} = \frac{1.6\times10^{-16}}{\sqrt{P_1}}$, giving the value of P_1. Absolute values of [N] are thus directly deducible from $I(580)$. Finally, with $G(\lambda)$ being known for every λ, the whole observed spectrum is intensity calibrated and all other P_i, $i = 2$ to 6 are obtained. This previously presented[b] calibration method is easier than the O_2 or NO titration methods.

Species Concentration

Pure N₂ Post Discharge

Figure 6 presents 1/[N] (simplified notation of 1/[N(⁴S)]) variation versus axial distance, which is linear, as expected.

[b] See J. Larbre, M. Ganciu, A.M. Pointu, M. Touzeau, J. Orphals, M. Vervloët, *Proc. Int. Workshop on Cold Atmospheric Pressure Plasmas Sources and Applications* Ghent, Belgium 2004, pp. 93–96.
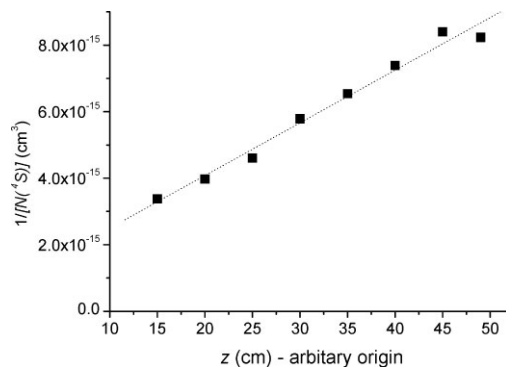

Figure 6. Linear variation of 1/[N(⁴S)] versus axial distance.

Figure 7 shows variations of [N(⁴S)] and [N(²P)] as a function of z (with an arbitrary origin). It is seen that they are roughly proportional, with a value of [N(²P)]/[N(⁴S)] ≈ 0.02.

The order of magnitude of [N₂(A)] can then be deduced from relations (9) and (10) in Table 1:

$$[N_2(A)] = (k_{10}/k_9) \times ([N(^2P)]/[N]) \times [N_2]$$
$$\approx 7 \times 10^{14} \text{ cm}^{-3} \qquad (15)$$

which is thus independent of z.

It must then be checked, a posteriori, that the convective term is negligible in the balance equation for [N(²P)], as compared to the source and loss terms corresponding to reactions listed in Table 1.

In fact, it seems that

$$V \times (1/[N(^2P)]) \times (d[N(^2P)]/dz)$$
$$\sim V \times (1/[N]) \times (d[N]/dz)$$
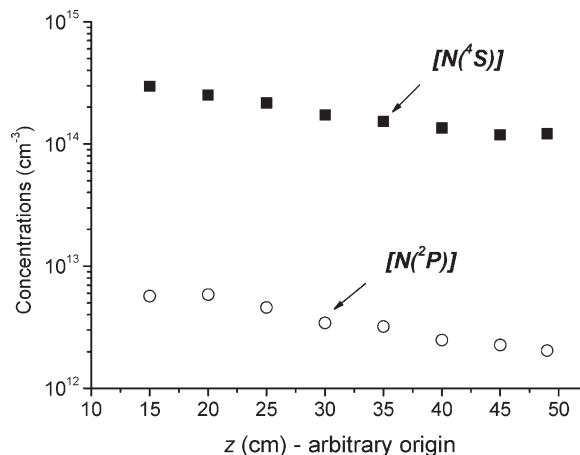$$= 2\alpha_{eff} \times [N] \times [N_2] \ll k_{10} \times [N_2] \qquad (16)$$

Figure 7. Concentrations versus axial distance of two measured N atomic states.

leading thus to the inequality

$$V \times d[N(^2P)]/dz \ll k_{10} \times [N(^2P)] \times [N_2] \qquad (17)$$

N₂ with O₂ Added as an Impurity

When a small amount of O₂ is added, the corresponding evolution of both [N(⁴S)] and [N(²P)] are shown in Figure 8, demonstrating that [N] = [N(⁴S)] decreases at fixed z for increasing [O₂], the variation of 1/[N] being always linear with z. In fact, as shown by measurements and modelling presented in ref. [10], linear extrapolation to higher z fails, and is replaced by an exponential increase of 1/[N], measured by a titration method in pure N₂ up to 3 m downstream of the discharge in a slightly thinner tube. A transposition to the conditions under study here should give $1/[N] \approx 5.7 \times 10^{-14}$ cm³ at 1.8 m.

Furthermore, all extrapolated straight lines converge to a unique point that can be identified as the source location, at z_0, where the corresponding value $[N]_0 = 1 \times 10^{15}$ cm⁻³ is independent of [O₂]. Despite the weakness of the forbidden line, it can be seen that a similar effect of O₂ occurs on the N(²P) species, as shown in Figure 9.

The increasing slope of 1/[N] versus z for increasing [O₂] corresponds to an increase of the apparent recombination coefficient α_{eff} of Equation (11) as illustrated in Figure 10.

Such an effect may involve the previously mentioned slope increase along with increasing values of the wall recombination probability γ, as calculated in ref. [10]. In ref. [19] a model is developed that shows that the γ value involves relative surface kinetics of N and O atoms and increases significantly with [O]/[N]. Here, although at higher pressure and with different wall material, an increase of [O₂] does increase [O] and could, therefore, induce similar effects. An alternative though not very probable explanation of the observed α_{eff} increase could be
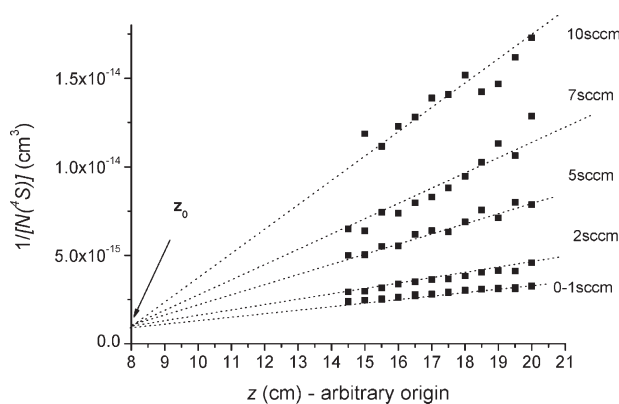

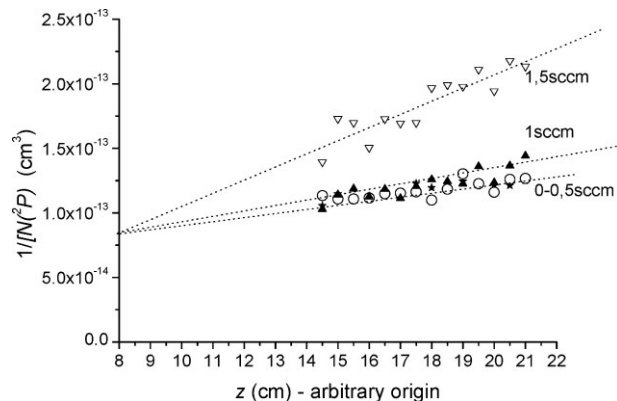Figure 9. Axial [N(²P)] variation with O₂ flow as a parameter ([O₂]/[N₂] = 2 × 10⁻⁵ × sccm).

a volume reaction of N with species Y, both due to O₂ and obeying [Y]/[N] = constant along z. Finally, it is possible that, the N + N recombination being a complex process in which all the N₂ (B, v′) states are concerned, the proportionality factor between [N]² and I(580) is not independent of the [O₂]/[N₂] ratio. A study of this possible latter effect is in progress.

Figure 11 presents, compared to [N], the variations of [O] and [O(¹S)] at z = 15 cm (arbitrary origin) as a function of O₂ flux. On the same figure, relative UV radiation, estimated through variation of the NO_γ line at 248 nm, is also presented.

Figure 12 shows that increasing the O₂ concentration drastically decreases [N₂(A)] (thus also [N(²P)] for quite constant [N]) up to the limit of the 346.6 nm line being unmeasurable.

Dominant active species are thus: i) N, N₂(A), and N(²P) in pure N₂, ii) N, N₂(A), N(²P), and O(¹S) with a small amount of added oxygen (around some 10⁻⁵ × [N₂]), iii) N and O. In the two latter cases, the UV NO_γ band is also present. Taking into account survival curves given in
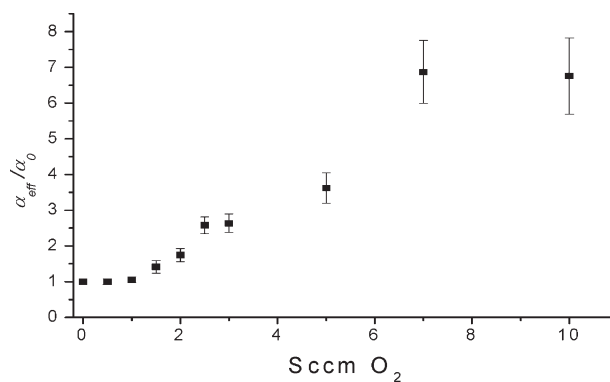

Figure 8. Axial 1/[N(⁴S)] variation with O₂ flow as a parameter ([O₂]/[N₂] = 2 × 10⁻⁵ × sccm).

Figure 10. Effect of O₂ on effective N volume recombination coefficient ([O₂]/[N₂] = 2 × 10⁻⁵ × sccm).
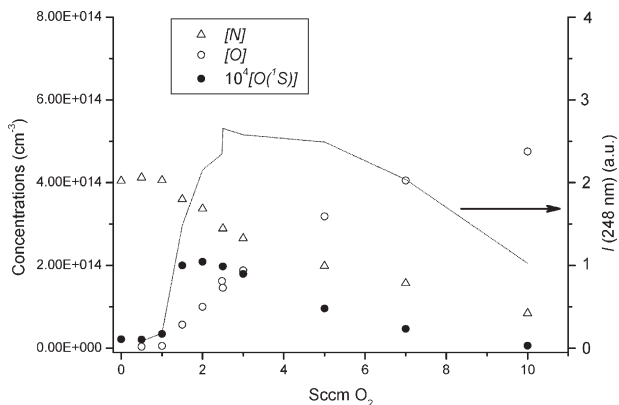
Figure 11. Nitrogen and oxygen atom concentrations and intensity of 248 nm NO_γ line versus O_2 impurity ($[O_2]/[N_2] = 2 \times 10^{-5} \times$ sccm) at fixed axial position $z = 15$ cm (arbitrary origin).

Figure 4, it appears that the biocidal effect is a result of N, $N(^2P)$, and $N_2(A)$ in pure nitrogen. This effect is increased with added O_2 to a maximum around 1 sccm, which reasonably follows the $[O(^1S)]$ variation. The intermediate biocidal efficiency obtained at 10 sccm could be attributed to the presence of UV light and of quite high O concentrations added to lowered [N].

Study of O(^{1}S) Kinetics

The source term, S, for the $O(^1S)$ state is generally (see ref. [20]) attributed to the reaction

$$O + N_2(A) \rightarrow O(^1S) + N_2 \qquad (18)$$

with $k_{18} = 2.1 \times 10^{-11}$ cm$^3 \cdot$ s^{-1},[18] which leads to:

$$S = k_{18} \times [O] \times [N_2(A)] \qquad (19)$$

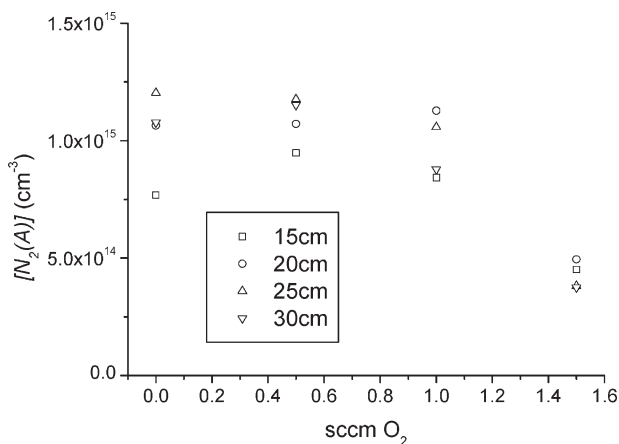The loss term is mainly quenching: i) by N_2 (source of radiating excimer $O(^1S).N_2$) with rate given by $q_1 \times [N_2] = 4 \times 10^{-18} \times [N_2]$ s^{-1},[15] and ii) by O_2, with rate $q_2 \times [O_2]$ (ref. [21] gives $q_2 = 2.56 \times 10^{-13}$ cm$^3 \cdot$ s^{-1}).

The total loss term is then

$$L = \{q_1 \times [N_2] + q_2 \times [O_2]\}[O(^1S)] = \kappa \times [O(^1S)] \qquad (20)$$

Taking into account axial convection, a concentration balance is written:

$$V \times d[O(^1S)]/dz = S - L$$
$$= k_{18} \times [O] \times [N_2(A)] - \kappa \times [O(^1S)] \qquad (21)$$

When S is quite constant around S_0 with negligible axial variation as compared to $S_0\kappa/V$, an approximated solution of Equation (21) is:

$$[O(^1S)] \sim S_0/\kappa + \{[O(^1S)]_0 - S_0/\kappa\}$$
$$\times \exp(-(-\kappa z/V) \qquad (22)$$

When such variation is verified, it is possible to determine S_0, $[O(^1S)]_0$, and κ. As an example, Figure 13, obtained for 2.5 sccm O_2 flux gives:

$$[O(^1S)]_0 = 5.9 \times 10^{10} \text{ cm}^{-3}, \ S = S_0$$
$$= 2.15 \times 10^{12} \text{ cm}^{-3} \cdot \text{s}^{-1}, \ \kappa = 281 \text{ s}^{-1}$$

Varying the O_2 flux allows observation of the corresponding κ variation, as shown in Figure 14. Under 2 sccm O_2 flux, [O] and consequently S increases sharply from zero, thus invalidating the $S = S_0$ assumption. Above 2 sccm, a linear variation range exists. This variation
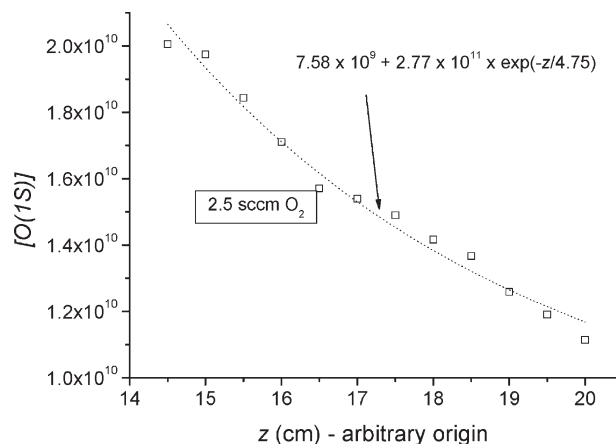

Figure 12. Metastable $N_2(A)$ concentration versus O_2 impurity ($[O_2]/[N_2] = 2 \times 10^{-5} \times$ sccm).

Figure 13. Experimental variation of $[O(^1S)]$ versus axial position z (arbitrary origin) fitted with exponential decrease for 2.5 sccm O_2 flux.
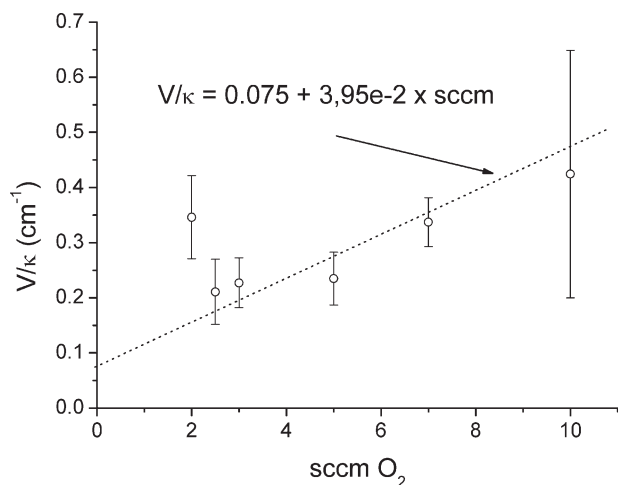
Figure 14. Flow velocity divided by the quenching rate of $O(^1S)$ as a function of O_2 flux.

corresponds to $\kappa = 100 + 8.7 \times 10^{-14} \times [O_2]$. When associated with $q_1 \times [N_2] + q_2 \times [O_2]$ it exhibits a very good agreement for q_1, and a disagreement by a factor 3 for q_2, both to be tempered by significant error bars.

S variation versus O_2 flux is shown in Figure 15, which shows a drastic decrease when O_2 increases. It is qualitatively coherent with a simultaneous decrease of both [O] and $[N_2(A)]$ but in quantitative disagreement with previously estimated concentrations at lower oxygen flux, if one uses relation (19). Besides the possibility of bad coefficient knowledge, other sources of $O(^1S)$ creation should be considered.

Discussion/Conclusion

A discharge afterglow flowing in a small inner diameter tube, of around 1 m in length, is shown to be able to
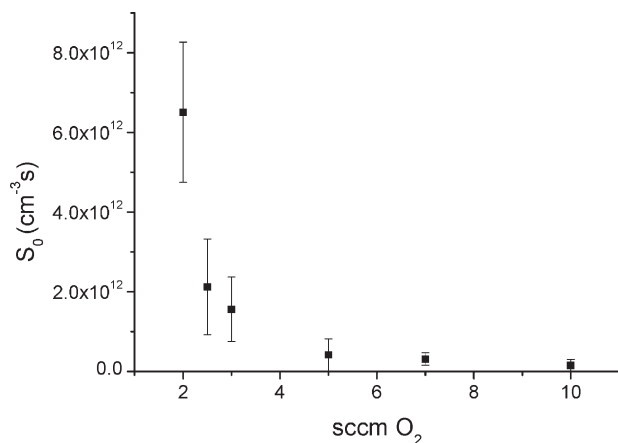

Figure 15. $O(^1S)$ source term as a function of O_2 flux.

produce significant biological deactivation. The gas is atmospheric pressure nitrogen, either pure or containing oxygen in very small proportion (some 10^{-5}). The deactivation is attributed to active molecular and atomic species. N, $N(^2P)$, $N_2(A)$, O, and $O(^1S)$, as well as NO (whose excited state, by the γ band, produces UV) have been identified as being present in the post discharge. Among these species, N, $N(^2P)$, and $N_2(A)$, reinforced by $O(^1S)$ with a small amount of added oxygen, are the species present when the measured biocidal effect is at a maximum. These species can transport their chemical energy over long distances, alongside possibly contaminated tube surfaces. Species concentration variation during transport is regulated by collision reactions and by visible and UV wavelength light emissions. Even at the end of the tube, these species are thought to have concentrations of the same order of magnitude as in the box used for the biological tests. This assumption is supported by the following considerations.

Let $\langle[N]\rangle$ be the [N] mean value in the biological test box. This box, volume τ, is fed at abscissa z by a gas flux Φ, and we assume that N losses are volume recombination with rate $2\alpha[N_2]$. The path of the gas flux within the box being long and complex, [N] at the box outlet is considered as negligible, compared to $[N](z)$, to then give:

$$\langle[N]\rangle^2 = [N](z) \times \Phi/(2\alpha[N_2]\tau) \qquad (23)$$

i.e., for experimental conditions, a value of $\langle[N]\rangle$ is comparable to [N] $(z > 1 \text{ m})$ at the tube outlet.

Such an approach also allows correlation of the biocidal effect in the box to $\langle[N]\rangle$ in the box. In a previous experiment mentioned in Section 3 performed with pure N_2 using a manuril tube connecting the plasma source to the biological test box, the biocidal effect was measured for 30 min exposure time and different tube lengths, ranging from 4 cm to 3 m. Using the same operating conditions, the value of [N] at the tube outlet was measured[9] and gives easily, using relation (23), an order of magnitude for $\langle[N]\rangle$ in the box. The biocidal effect and estimated $\langle[N]\rangle$ values as a function of the tube length are reported in Figure 16. As a matter of fact, it appears that the spore population reduction decreases when the tube length increases, and consequently when the estimated $\langle[N]\rangle$ in the box decreases. This is consistent with the present results.

Moreover, special attention has been paid to $O(^1S)$ which appears to contribute to the biocidal effect. Through study of how it is transported along the tube, quenching with N_2 and O_2 has been shown to be a major loss mechanism. Simultaneously optimizing the source term appears to imply a very low oxygen partial pressure, with a maximum of $O(^1S)$ concentration for an oxygen-to-nitrogen ratio of around 5×10^{-5}, a value compatible
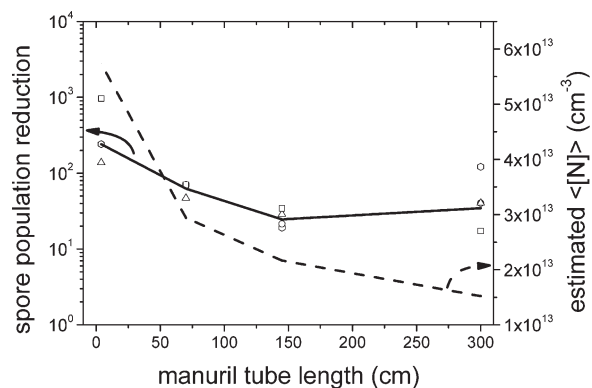
Figure 16. B. stearothermophilus spore population reduction in pure nitrogen post discharge and mean [N] in the biological test box as a function of manuril tube length connecting the plasma source and the box; 30 min. exposure time; exposed population: 2.6×10^4.

with air leak conditions in pure N_2. This can be compared to a very recent study[22] that shows that the N_2 afterglow of a commercially available reactor produces $O(^1S)$ metastable density about 3 to 4 times less than in the present conditions. This is attributed to air, which is present as an impurity in the N_2 gas.

Finally, the studied species contribute, either directly or indirectly, to the measured biocidal effect, making the device under study a good candidate to decontaminate the inner surface of medical tubes.

In addition, the observed innocuousness relative to the polyurethane wall constitutes a desired feature.

The societal importance of the decontamination subject makes welcome any and all progress toward a solution, even as a step towards an eventual sterilization process. Transportation over long distances of active species that are not chemically or thermally aggressive to polymeric material but with a proven biocidal effect constitutes one such solution.

[1] E. Stoffels, A. J. Flikweert, W. W. Stoffels, G. M. W. Kroesen, *Plasma Sources Sci. Technol.* **2002**, *582*, 383.
[2] M. Laroussi, C. Tendero, X. Lu, S. Alla, W. L. Hynes, *Plasma Process. Polym.* **2006**, *3*, 470.
[3] G. Friedman, M. Peddinghaus, M. Balasubramanian, H. Ayan, A. Fridman, A. Gustol, A. Brooks, *Plasma Chem. Plasma Process.* **2006**, *26*, 425.
[4] J. Pollak, M. Moisan, D. Kéroack, J. Séguin, J. Barbeau, *Plasma Process. Polym.* **2008**, *5*, 14.
[5] M. J. Kirkpatrick, B. Dodet, E. Odic, *Int. J. Plasma Environ. Sci. Technol.* **2007**, *1*, 96.
[6] M. Ganciu, J. Orphal, M. Vervloët, A. M. Pointu, M. Touzeau, *Bull. Am. Phys. Soc.* **2002**, *47*, 29.
[7] A. M. Pointu, A. Ricard, B. Dodet, E. Odic, J. Larbre, M. Ganciu, *J. Phys D: Appl. Phys.* **2005**, *38*, 1905.
[8] US 7 229 589 (2007), invs.: M. Ganciu-Petcu, A. M. Pointu, B. Legendre, J. Orphal, M. Vervloet, M. Touzeau, N. Yagoubi.
[9] M. Ganciu, J. Orphal, A. M. Pointu, M. Vervloet, *Chem. Phys. Lett.* **2005**, *413*, 468.
[10] P. Fromy, A. M. Pointu, M. Ganciu, J. Orphal, *J. Phys. D: Appl. Phys.* **2006**, *39*, 108.
[11] L. G. Piper, L. M. Cowles, *J. Chem. Phys.* **1986**, *85*, 2419.
[12] M. Simek, *Plasma Sources Sci. Technol.* **2003**, *12*, 421.
[13] L. G. Piper, T. R. Tucker, W. P. Cummings, *J. Chem. Phys.* **1991**, *94*, 7667.
[14] C. D. Pintassilgo, J. Lourreiro, V. Guerra, *J. Phys. D: Appl. Phys.* **2005**, *38*, 417.
[15] G. Black, R. L. Sharpless, T. G. Slanger, *J. Chem. Phys.* **1975**, *63*, 4546.
[16] J. F. Noxon, *J. Chem. Phys.* **1962**, *36*, 926.
[17] V. Guerra, E. Tatarova, C. M. Ferreira, *Vacuum* **2002**, *69*, 171.
[18] A. Kossyi, A. Yu Kotinsky, A. A. Matveyev, V. P. Silakov, *Plasma Sources Sci. Technol.* **1992**, *1*, 207.
[19] B. Gordiets, C. M. Ferreira, J. Nahorny, D. Pagnon, M. Touzeau, M. Vialle, *J. Phys. D: Appl. Phys.* **1996**, *29*, 1021.
[20] N. Gherardi, G. Gouda, E. Gat, A. Ricard, F. Massines, *Plasma Sources Sci. Technol.* **2000**, *9*, 340.
[21] E. C. Zipft, *Geophys. Res. Lett.* **1979**, *6*, 881.
[22] A. Ricard, E. Panousis, F. Clement, T. Sindzingre, J. F. Loiseau, *Eur. Phys. J. Appl. Phys.* **2008**, *42*, 6363.